Journal of Immunological Methods 428 (2016) 20–29

Contents lists available at ScienceDirect

Journal of Immunological Methods

journal homepage: www.elsevier.com/locate/jim

# Analyses of movement and contact of two nucleated cells using a gas-driven micropipette aspiration technique

Hao Yang [1], Chunfang Tong [1], Changliang Fu, Yanhong Xu, Xiaofeng Liu, Qin Chen, Yan Zhang, Shouqin Lü, Ning Li, Mian Long *

*Key Laboratory of Microgravity (National Microgravity Laboratory), Center of Biomechanics and Bioengineering, and Beijing Key Laboratory of Engineered Construction and Mechanobiology, Institute of Mechanics, Chinese Academy of Sciences, Beijing 100190, China*

ARTICLE INFO

*Article history:*
Received 21 July 2015
Received in revised form 6 October 2015
Accepted 18 November 2015
Available online 2 December 2015

*Keywords:*
Nucleated cells
Movement
Contact
Adhesion
Pipette

ABSTRACT

Adhesion between two nucleated cells undergoes specific significances in immune responses and tumor metastasis since cellular adhesive molecules usually express on two apposed cell membranes. However, quantification of the interactions between two nucleated cells is still challenging in microvasculature. Here distinct cell systems were used, including three types of human cells (Jurkat cell or PMN vs. MDA-MB-231 cell) and two kinds of murine native cells (PMN vs. liver sinusoidal endothelial cell). Cell movement, compression to, and relaxation from the counterpart cell were quantified using an in-house developed gas-driven micropipette aspiration technique (GDMAT). This assay is robust to quantify this process since cell movement and contact inside a pipette are independent of the repeated test cycles. Measured approaching or retraction velocity follows well a normal distribution, which is independent on the cycle period. Contact area or duration also fits a Gaussian distribution and moreover contact duration is linearly correlated with the cycle period. Cell movement is positively related to gas flux but negatively associated to medium viscosity. Cell adhesion tends to reach an equilibrium state with increase of cycle period or contact duration. These results further the understanding in the dynamics of cell movement and contact in microvasculature.



## 1. Background

Blood cells undergo the flow-driven movement in the circulation and encounter the other flowing blood cells or tumor cells or endothelial cells. This process leads to forming cell–cell contact and even aggregation or adhesion mediated by receptor–ligand pairs expressed on the respective surfaces of two apposed cells. Under physiological flow, the cell movement, contact, and aggregation or adhesion are quite sophisticated, since a huge population of homotypic or heterotypic cells interacts with each other inside a blood vessel and a vast variety of receptor or ligand molecules and the complexity of flow patterns are involved. For example, flowing leukocytes in the blood stream usually collide with other cells, and periodically become aggregated with blood cells or tumor cells, or adhere to endothelial cells mediated by the cellular adhesive molecules such as selectins or integrins with their corresponding ligands (Ley, 2003; Li et al., 2012). While the limited in vivo data has been collected using different approaches such as intravital microscopy, in vitro approaches are also required to elucidate the detail information for these processes.

Various in vitro approaches are well developed to understand the above processes. For example, a cone-plate viscometer assay was used to monitor the time course of cell movement and aggregation under a simple shear flow in a type of population study (Tees and Goldsmith, 1996; Long et al., 1999; Liang and Dong, 2008). A single cell pair study was also conducted using a micropipette suction assay to define the tether force and the adhesion probability between a moving cell inside one pipette and the other cell sucked by another pipette (Gelles et al., 1988; Shao and Xu, 2002; Chesla et al., 1998; Huang et al., 2004). Notably, it is hard to collect all the physiologically-relevant information of cell movement, contact, and aggregation or adhesion in a single assay mentioned above. Meanwhile, some of these assays are less biologically relevant since those receptors or ligands have been purified from the native cells and then coated on a force transducer cell (i.e., a human red blood cell (RBC) (Chesla et al., 1998; Huang et al., 2004). Recently, we developed a novel gas-driven micropipette aspiration technique (GDMAT) to manipulate the adhesion of two nucleated cells mediated by the constitutively-expressed receptor–ligand binding, which could not be determined in a conventional MAT technique upon membrane deflection. This assay has been used to quantify the adhesion kinetics of polymorphonuclear neutrophils (PMN) expressing $\beta_2$-integrins to the endothelial cells (Human pulmonary microvascular endothelial cell (HPMEC)) or tumor cells (melanoma cell WM9 or breast cancer cell MDA-MB-231) bearing intercellular adhesion molecule 1 (ICAM-

* Corresponding author at: Institute of Mechanics, Chinese Academy of Sciences, Beijing 100190, China.
*E-mail address:* mlong@imech.ac.cn (M. Long).
[1] The authors contributed equally to this work.

http://dx.doi.org/10.1016/j.jim.2015.11.007
0022-1759/

1) ligands (Fu et al., 2011). Moreover, this GDMAT assay also provides an opportunity to refine the cell movement, contact, and adhesion inside a pipette.

To further develop this assay as a widely applicable, robust approach for nucleated cells, it is required to quantify the impact of those potential regulating factors on cell movement, contact, and adhesion in well-defined data analysis procedures. Several issues need to be properly addressed: 1) *Cell movement inside the pipette*. This is associated with several parameters such as positive pressure driven by gas flow, negative pressure exerted by hydraulic suction, pipette diameter, smoothness of pipette wall via pre-coated biomolecular layers, medium viscosity, cell morphology, cell surface topology, and mechanical feature of the cell. Obviously, these parameters govern the potential jerkiness of approaching or retraction movement inside the pipette. 2) *Cell contact at the tip of the pipette*. Effects of gas-flow-induced impinging force on cell adhesion are as similarly important as the suction pressure-mediated pulling force for a RBC in conventional MAT measurement. In *compression* phase, the topology and mechanics of molecular carrier (i.e., the moving cell) are potentially related to the impinging force, contact area, and contact duration. They may also be critical in *relaxation* phase to determine the adhesion event and then the adhesion probability, since some receptor–ligand bonds could be broken up due to the "jerkiness" during the relaxation and, thus, may be undetectable. 3) *Determination of adhesive events*. The fate of one cell–cell contact event is defined by the change of retraction velocity at a single test cycle. Image digitalization and point-by-point positioning techniques at reasonably low computing cost, as well as well-defined displacement calculation and detail statistical analysis are required to enhance the accuracy of data collection and to improve the criteria of determination of an adhesive event. Meanwhile, consecutive test cycles are required to determine the time course of adhesion probability, but it is still little known whether and/or how the presence of an adhesion, tether, or non-specific binding event in one test cycle affect the outcome from the next cycle in the sequentially repeated cycles. Specifically, membrane tether is one type of adhesion event but is difficult to distinguish them from the nonspecific events especially when the moving cell interacts with pipette wall (Long et al., 1999; Wu et al., 2007).

In this work, we conducted the detail dynamic analyses for a nucleated cell moving inside a pipette and interacting at the pipette tip with a counterpart nucleated cell held by another pipette. Approaching or retraction velocity and contact area or duration were determined for various cells under distinct conditions. Independence of different regulating factors on cell adhesion was discussed. Our results indicated that the new assay is well applicable to analyze the dynamics of cell movement and contact inside a size-limited pipette.

## 2. Methods

### 2.1. Reagents and cell culture

Mouse IgG anti-human monoclonal blocking antibodies (mAbs) against $\alpha_L$ chain (CD11a, clone MEM-25) were purchased from Invitrogen (Carlsbad, CA). Mouse IgG anti-human blocking mAbs against $\alpha_M$ chain (CD11b, clone 44) were from Chemicon International (Temecula, CA). Mouse IgG anti-human blocking mAbs against $\beta_2$ chain (CD18, clone 212701) and ICAM-1 (CD54, clone BBIG-I1 (11C81)) were from R&D System (Minneapolis, MN). Allophycocyanin APC-conjugated anti-mouse Ly-6G/Ly-6C (Gr-1) antibodies (clone RB6-8C5) or fluorescein isothiocyanate (FITC)-conjugated rat anti-mouse CD146 antibodies (clone ME-9F1) were purchased from Biolegend (Santiago, CA).

Human acute T cell leukemia cell line Jurkat (obtained from ATCC, Rockefeller, USA) were grown in RPMI-1640 medium supplemented with 1 mM L-glutamine, 100 units/ml penicillin, 10 μg/ml streptomycin, and 10% fetal bovine serum (FBS). To conduct the adhesion probability measurements, the cells were suspended in Hank's balanced salt solution (HBSS) with $Ca^{2+}$ and $Mg^{2+}$ containing 10 mM 4-(2-Hydroxyethyl)piperazine-1-ethanesulfonic acid (HEPES) and 4% FBS.

Fresh human PMNs (hPMNs) were obtained from whole blood samples collected by venipuncture and then isolated using a Ficoll density gradient (Histopaque-1077 and Histopaque-1119 from Sigma). Collected cell mixture with ~20–50% of hPMNs was kept at 4 °C in Dulbecco's phosphate-buffered saline (D-PBS) containing 0.1% human serum albumin (HSA) for up to 4 h (Tees and Goldsmith, 1996). Individual hPMNs were directly used for adhesion probability assays without further lysing RBCs from cell mixture in order to minimize the activation of hPMNs. For blocking measurements, the cells were pre-incubated with combined anti-$\alpha_L$, -$\alpha_M$, and $\beta_2$ blocking mAbs at a concentration of 10 μg/ml for 45 min on ice. To conduct the adhesion probability measurements, the cells were suspended in HBSS with $Ca^{2+}$ and $Mg^{2+}$ containing 10 mM HEPES and 4% FBS.

Human metastatic breast adenocarcinoma cell line MDA-MB-231 (purchased from Cell Culture Center of Union Medical University, Beijing, China) was cultured in L-15 medium supplemented with 1 mM L-glutamine, 100 units/ml penicillin, 10 μg/ml streptomycin, and 10% FBS. For adhesion probability measurement, confluent cells were trypsinized and washed twice with fresh medium. Collected cells were then re-suspended in the medium and allowed to recover for 1 h while being rocked at 80 rpm at 37°C. For blocking measurements, the cells were pre-incubated with anti-ICAM-1 blocking mAbs at a concentration of 10 μg/ml for 45 min on ice. To up-regulate the expression of ICAM-1, the cells were incubated with TNF-α (R&D system) at respective 110 and 300 units/ml for 24 h before use.

Mouse PMNs (mPMNs) were obtained from peripheral blood samples collected via mouse eyes. The sample was centrifuged at 1600 rpm for 10 min, lysed twice with 1× RBC lysis buffer for 5 or 3 min, washed once with 5 ml staining buffer, and finally re-suspended with 100 μl staining buffer. Collected mPMNs were incubated with APC-conjugated mouse Ly-6G/Ly-6C (Gr-1) mAbs for 45 min at 4°C before flow cytometry sorting. Sorted mPMNs were kept in DPBS solution with 4% FBS at 4°C before use.

Mouse liver sinusoidal endothelial cells (LSECs) marked with FITC-conjugated CD146 mAbs were purified from the non-parenchymal cells (NPCs) by flow cytometry sorting. Briefly, the liver from an anesthetized mice was perfused at 5 ml/min for 5 min with a balanced salt solution containing heparin and ethylene glycol tetraacetic acid (EGTA) through hepatic portal vein, followed with 25 ml of 4 mM $CaCl_2$, 0.5% BSA, 2% FBS and 0.05% collagenase IV (from Sigma) in high glucose Dulbecco's modified Eagle's medium (DMEM) at 5 ml/min. The liver was then minced and stirred in 10 ml high glucose DMEM with 14 μg/ml DNAse, 4.3 mM $MgCl_2$, 0.05% bovine serum albumin (BSA) and 2% FBS at 37°C at pH 7.4 for 10 min and then centrifuged at 54 ×*g* for 1 min twice for collecting the supernatant, followed with 500 ×*g* for 8 min twice for collecting the sediment which were then re-suspended for a density gradient equilibrium centrifugation. Mouse NPCs were collected from layers between 11% and 17.6% Optiprep™ (from Alix) density gradient after centrifugation at 4°C for 18 min at 1400 ×*g*. NPCs were re-suspended in 14 ml staining buffer solution and centrifuged at 500 ×*g* for 10 min before being stained with FITC-conjugated CD146 mAbs in 100 μl staining buffer solution for 45 min. Sorted LSECs were recovered in high glucose DMEM with 10% FBS, 100 units/ml penicillin, 10 μg/ml streptomycin and 1 mM L-glutamine by shaking at 4°C for 1 h at 100 rpm before use.

### 2.2. Ethics and consent statement

All the protocols with human and mouse samples were approved by the Institutional Review Board for Animal and Medicine Ethical Committee of the Institute of Mechanics, Chinese Academy of Sciences. Likewise, adult participants in the study provided the informed consent for blood donation.

### 2.3. Gas-driven micropipette aspiration technique

The GDMAT approach was described previously for quantifying the interactions of two nucleated cells bearing respective receptors and ligands (Fu et al., 2011). Briefly, a gas-driven pressure unit was added into a conventional MAT system (Huang et al., 2004; Wu et al., 2007). To manipulate the forward and backward movement of a cell inside the left pipette, a positive pressure was exerted by the pressure unit via controlling gas flux gauged by a pressure regulator while a negative pressure was applied by the conventional suction via adjusting the height of reservoir gauged by a micrometer, resulting in a test cycle of cell approaching to, contacting with, and withdrawing from the counterpart cell held steadily in the right pipette (Fig. 1A; Fig. 1C). Switch between positive and negative pressures was implemented via a solenoid valve at a time relay of 3 s in one test cycle and repeated automatically the approach–contact–retraction cycles at a given cycle period, *T*. The images of cell movement were recorded in a compressed MPEG-2 format (720 × 576 pixels, 25 frames per second) using a CCD camera (WAT-902 H, Watec, Japan) and then decoded using a video encoder board (MP-400, Gotron, China). The moving distance of the cell inside the pipette was calibrated at a resolution of ~74.6 nm per pixel using a standard micro-ruler, and the time course of cell movement and cell–cell contact was analyzed off-line frame-by-frame.

To understand the cell movement and contact dynamics, several parameters were systematically varied including gas flux, cycle period, as well as the medium viscosity in this work. Meanwhile, the calibration curve between gas flux and suction pressure was determined independently by systematically varying the suction pressures and accordingly adjusting the gas fluxes (Fu et al., 2011).

### 2.4. Analysis of cell movement and contact inside pipette

We started with analyzing the free-flow of a cell inside the pipette. Assuming that no interactions exist between the moving cell and other flowing cells or the pipette wall and that the density gradient between the cell and the medium is trivial (i.e., the density of a PMN, $\rho_c$, is ~1.08 kg/L), the cell is forced by positive pressure-induced fluid flow to move along the pipette and follows the law of Hagen–Poiseuille. The velocity of incompressible viscous fluid at the pipette axis at time *t*, $U_f(t)$, in an infinitely long, uniform cross-sectioned tube is given by (Langlois and Deville, 2014),

$$U_f(t) = \frac{GR_p^2}{4\mu} - \frac{2GR_p^2}{\mu}\sum_{n=1}^{\infty}\frac{1}{k_n^3 J_1(k_n)}\cdot \exp\left(-k_n^2 \mu t/\rho_c R_p^2\right), \quad (1)$$

where *G* is the pressure gradient ($= \Delta p^f/L$ where $\Delta p^f$ and *L* are the respective positive pressure and limited length), $R_p$ and μ are the pipette radius and the medium viscosity, respectively, and $J_1(k_n)$ and $k_n$ are the first-order Bessel function and the eigenvalue of zero-order Bessel function, respectively. The first right term denotes the fully-developed pipette fluid, on which the free-flow velocity of the cell in the pipette, $U_f(t)$, can be calculated using the limited length, the radius, the medium viscosity, and the positive pressure. The second term on the right defines the initiating phase of pipette flow, which can be neglected since the flow quickly reaches the steady flow in a few seconds in the current study.

Once encountering with the counterpart cell sucked steadily by another pipette (Fig. 1A; C), the moving cell is impinged finitely and kept steady for a preset duration. After relaxing back by the applied suction pressure $\Delta p^w$, the cell finally moves away from the counterpart cell by undergoing an initially accelerating phase in short time and quickly reaching the terminal velocity of free-flow (Fig. 1B), which is governed by a similar formulation of Eq. (1) (only difference comes from the pressures $\Delta p^f$ and $\Delta p^w$ that are controlled separately). Any arbitrary contact of the two cells results in the fate of no adhesion, adhesion without tether bond, or tether bond formation, which determines distinct magnitude and duration of the accelerating phase (Fu et al., 2011).

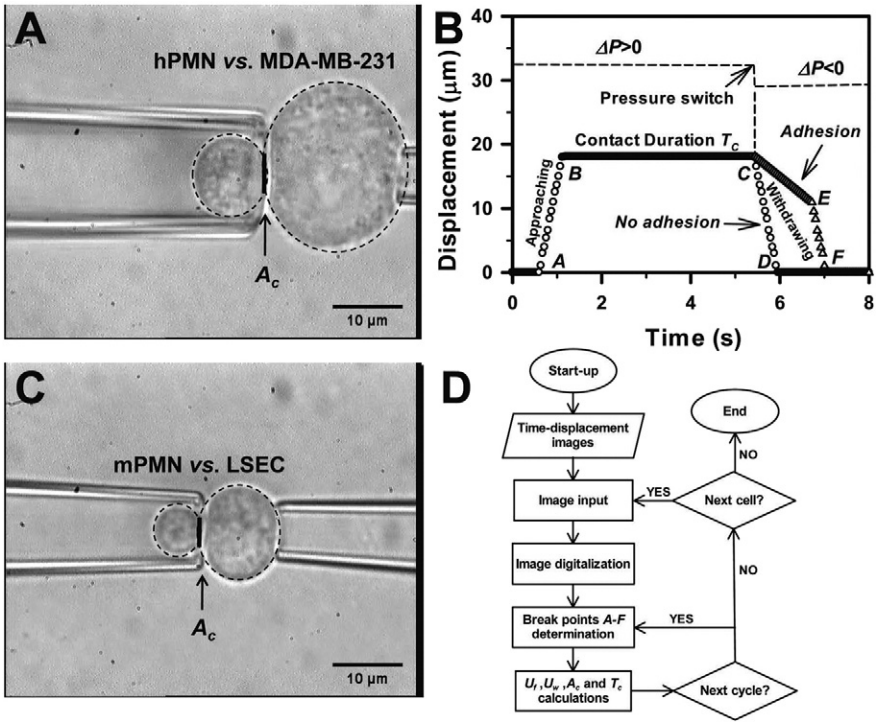


**Fig. 1.** Analysis of cell movement and contact inside pipette. Optical image of cell contact between a hPMN (*A*) or a mPMN (*C*) (moving inside *left* pipette) and a human MDA-MB-231 or a mouse LSEC cell (steadily sucked by *right* pipette) using a gas-driven micropipette aspiration technique (GDMAT). Also plotted is the typical displacement of the moving cell, as shown in *A*, with time in a single test cycle (*B*). Panel *D* illustrated the flowchart of image processing and parameter determination via defining the break points *A–F* shown in *C*.

### 2.5. Data analysis

To determine the related dynamic features, the time course of cell movement inside the pipette was monitored in the entire approach–contact–retraction cycle and measured frame-by-frame upon a simplified direct-search protocol (Fig. 1B; D). The resulting displacement spectrum enabled us to determine the approaching velocity, $U_f$, apparent contact area, $A_c$, contact duration, $T_c$, and retraction velocity, $U_w$, of the moving cell in each test cycle and to lump these parameters together from repeated cycles per cell pair. 2–5 cell pairs were tested in each case and 30–50 cycles were repeated for each cell pair (Fig. 1D). It was noted that the spectrum was also able to identify the occurrence of an adhesion event for a nucleated cell since the membrane deflection on cell tip was no longer visible when the nucleated cell was withdrawn (Fu et al., 2011). A Pearson correlation analysis (Mansson et al., 2004) was used to test the interplay for the same parameter in the sequential cycles, while a cross-correlation method (Gelles et al., 1988; Shao and Xu, 2002; Sun et al., 2009a, 2009b) was applied to test the relationship of the paired parameters between $U_f$ and $U_w$ or $A_c$ and $T_c$. A Student *t*-test was also performed for the measured parameters of $U_f$, $U_w$, $A_c$, or adhesion probability, and presented in different significance levels ($^*$, $P < 0.05$; $^{**}$, $P < 0.01$; $^{***}$, $P < 0.005$).

## 3. Results

### 3.1. Independence of cell movement on consecutive test cycles

The freely-moving cell was compressed a little (*upswept segment*) when it was forced by positive pressure to contact with another cell, but the adhered cell recoiled slightly (*deflexed segment*) when a negative pressure was imposed with a quick response less than one frame time (Fig. 1B). But it is unknown whether the compression and relaxation in one test cycle place any effects on the cell movement and contact in the consecutive cycle, especially when cell adhesion occurs and the relaxation duration is governed by the length of microvillus, the strength of receptor–ligand bond, as well as the cell deformation generated by the impinging force. To test this potential effect, test cycle dependence of cell movement on consecutive cycles was evaluated for Jurkat or hPMN vs. MDA-MB-231 and mPMN vs. LSEC cell systems at given cycle periods. Data indicated that both the approaching ($U_f$) and retraction ($U_w$) velocities slightly fluctuated but yielded comparable values for the two types of PMNs up to thirty consecutive cycles at typical periods of $T = 10$ and 12 s (Fig. 2A–B), suggesting that the cell movement is independent of test cycle sequence. This observation was further confirmed by a Pearson correlation analysis that either $U_f$ or $U_w$ is unlikely correlated in consecutive cycles (Fig. S1A–B). By contrast, a cross-correlation analysis indicated that $U_f$ and $U_w$ was highly correlated at the same cycle with the correlation coefficient of 0.80–1.00 for all the cases. These results implied that the compression and relaxation of the moving cell, when approaching to and withdrawing from the steady cell, have little impacts on cell movement inside a pipette.

### 3.2. Distribution of cell moving velocity on varied cycle periods

Not only the cell movement is independent of repeated test cycles at a single given cycle period, but the cell also moves stably at systematically-varied cycle periods in distinct cases of cell adhesion. Here the dependence of freely-moving velocity on cycle period was first compared when an intact hPMN was driven to approach to and withdraw from a MDA-MB-231 cell. Mean moving velocity was obtained from the data of 2–5 cell pairs in 30–50 cycles each pair. At eight given cycle period $T = 8$, 10, 12, 15, 18, 22, 26, and 31 s, mean approaching velocity yielded 21.9–35.4 μm/s and decreased slightly with increased cycle period (Fig. 3A), but no differences were found except of those between 12 and 31 s. Comparably, mean retraction velocity was similar at distinct cycle periods and valued 31.1–51.4 μm/s (Fig. 3B). Indifferences in approaching or retraction velocities were also observed between the hPMNs pre-incubated with combined anti-$\alpha_L$, -$\alpha_M$, and $\beta_2$ blocking mAbs and the MDA-MB-231 cells pre-incubated with anti-ICAM-1 blocking mAbs which abolish the $\beta_2$-integrin-ICAM-1-mediated adhesion ($U_f = 28.8$–39.3 and $U_w = 34.7$–42.0 μm/s) (Fig. 3C–D), or between the intact hPMNs and the MDA-MB-231 cells pre-stimulated by TNF-α which enhances the ICAM-1 expressions and, in turn, foster the adhesion ($U_f = 28.1$–42.9 and $U_w = 35.7$–45.6 μm/s) (Fig. 3E–F). These results indicated that mean freely-moving velocity of a hPMN is likely independent on varied cycle period when the cell interacts with a MDA-MB-231 cell in the cases of native, down-regulated, or up-regulated adhesion.

We further tested the distribution of estimated velocities at given periods. In a typical case of $T = 18$ s, both approaching (*solid bars*) and retraction (*open bars*) velocities followed a normal distribution in all the three cases of a hPMN interacting with a MDA-MB-231 cell (Fig. 4A–C). Fitting these data well with a Gaussian equation imparted the normally-distributed feature (*lines*) in a reasonable correlative coefficient and returned the predicted mean value of $x_0 = 20.6$–37.1, 20.3–42.7, and 28.5–37.0 μm/s for cell approaching or $x_0 = 27.6$–43.0, 37.3–49.8, and 30.7–44.6 μm/s for cell retraction (Tables 1; Table S1; Table S2). As expected, the predictions $x_0$ were in agreement with

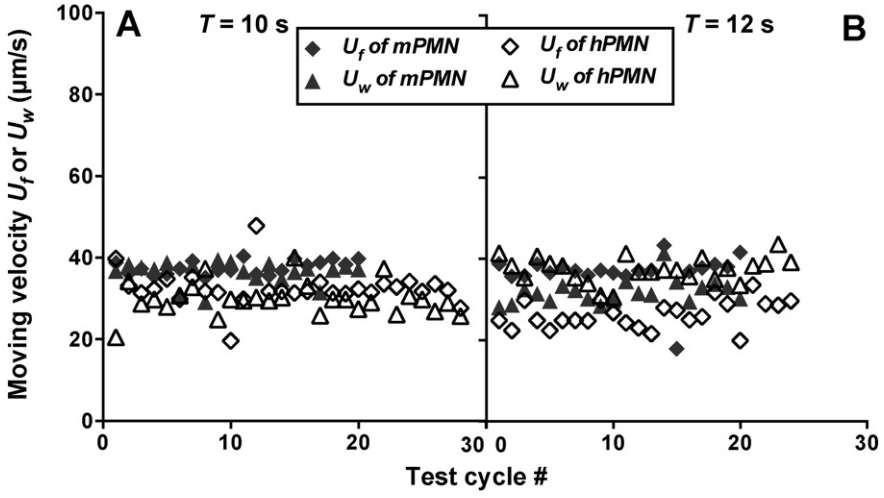


**Fig. 2.** Dependence of cell movement on consecutive test cycles. Dependence of cell freely-moving velocity, $U_f$ (*diamonds*) or $U_w$ (*triangles*), on consecutive cycles at two typical cycle periods of 10 (*A*) and 12 (*B*) s when a hPMN (*open points*) or a mPMN (*solid points*) approaches to and withdraws from a human MDA-MB-231 cell or a mouse LSEC cell, respectively.

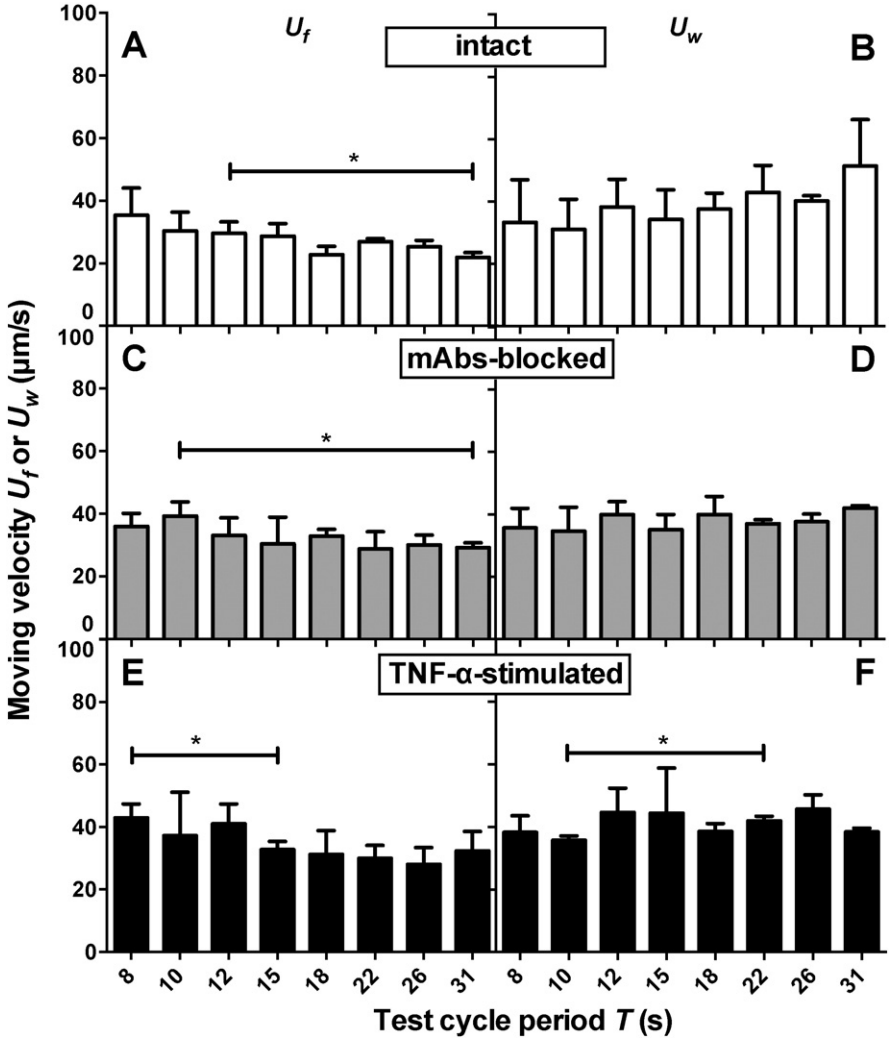


**Fig. 3.** Distribution of cell moving velocity on varied cycle periods. Dependence of freely-moving velocity, $U_f$ (*A*, *C*, *E*) or $U_w$ (*B*, *D*, *F*) on cycle period, when a hPMN approaches to or withdraws from a MDA-MB-231 cell in an intact (*A*, *B*), mAbs-blocked (*C*, *D*), or TNF-α-stimulated (*E*, *F*) case. Data were presented as the mean ± standard deviation (SD) of moving velocity for ≥5 cycles per cell pair for 2–5 cell pairs in each case, and compared with their statistical differences between any two of eight cycle periods.

those measured mean values of $U_f$ or $U_w$. Only quite a few distributions are exceptional with a low coefficient or even not Gaussian distribution (cf. Tables 1; Table S2). Taking the mean (Fig. 3; Tables 1; Table S1; Table S2) and distributed (Fig. 4) values together, these data indicated that both approaching and retraction velocities are normally distributed at a given cycle period and retain the similar values from one to another cycle period. Extra readout that the approaching velocity seems lower than the retraction velocity at long cycle periods was mainly because both the gas-driven approaching phase and suction pressure-driven retraction phase were driven by distinct action patterns and not able to make the quantitative comparison between the two velocities directly.

### 3.3. Stability of cell–cell contact

In addition to analyzing the approaching and retraction dynamics of cell free movement inside the pipette, we also tested the dependence of apparent contact area $A_c$ and contact duration $T_c$ on consecutive cycles when a hPMN or a mPMN made contact to a MDA-MB-231 or a LSEC cell. At a typical period of $T = 10$ s, either $A_c$ or $T_c$ was comparable up to twenty consecutive cycles (Fig. 5A), indicating that cell contact is stable and not varied with test cycles. Again, a Pearson correlation analysis indicated that either $A_c$ or $T_c$ is unlikely correlated in consecutive cycles (Fig. S1C–D). By contrast, a cross-correlation analysis indicated that $A_c$ and $T_c$ were highly correlated at the same cycle with the correlation coefficient of 0.77–1.00 for all the cases.

Moreover, the dependence of contact duration, $T_c$, on cycle period, $T$, was analyzed in the intact, mAbs-blocked, and TNF-α-stimulated cases. Here the values of contact duration for all the test cycles collected from 2–5 cell pairs in each case were averaged and plotted against given cycle periods. It was seen that the two parameters are linearly correlated (*points* in Fig. 5B). A linear equation, $T_c = aT + b$, fitted well the data (*lines* in Fig. 5B), which returned the similar values of the slope ($a$ = 1.08–1.24) and the intercept ($b = -6.19$–$-5.55$ s). The negative value of the intercept is not surprised since the ratio of the absolute value of the intercept to the slope, $|b|/a$, defines the actual mean time interval (4.48–5.73 s) for the free movement of a hPMN inside the pipette within a test cycle. Similar results were found for the binding of a mPMN to a LSEC (*solid points* in Fig. 5B). These data indicated that the gas-driven cell–cell contact is statistically stable no matter if PMNs are intact or mAbs-blocked, or MDA-MB-231 cells were intact, mAbs-blocked or TNF-α-stimulated.

We further tested the distributions of the resulting contact area and contact duration at given periods in the respective intact, mAbs-blocked, and TNF-α-stimulated cases. At a typical $T = 18$ s, either $A_c$ (Fig. 6A) or $T_c$ (Fig. 6B) most likely followed a normal distribution (*bars*). Fitting these data well with a Gaussian equation imparted the normally-distributed feature (*lines*) in a high correlative coefficient and

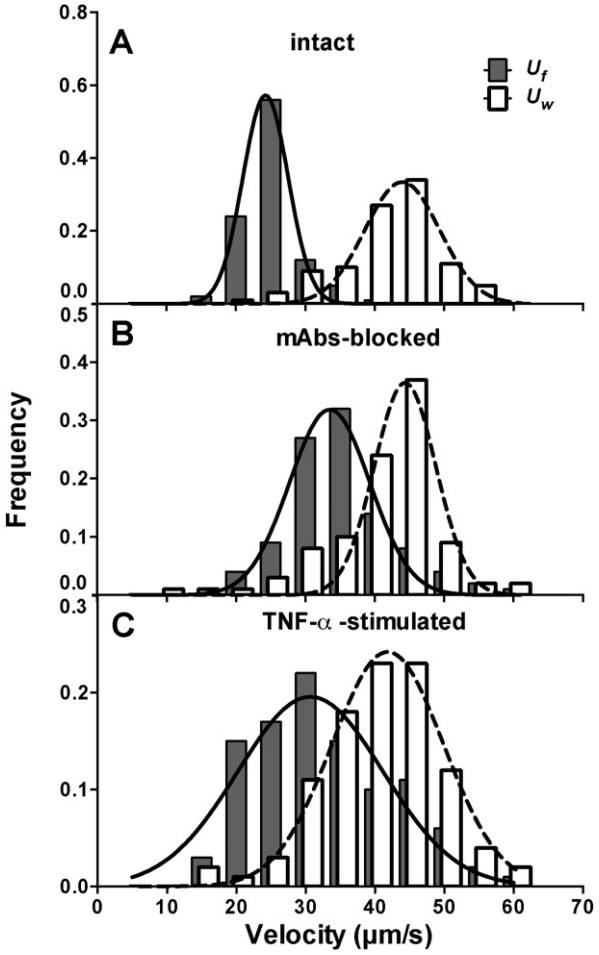


**Fig. 4.** Distribution of moving velocities at given periods. Typical distributions of cell velocity, $U_f$ or $U_w$, when a hPMN approaches to or withdraws from a MDA-MB-231 cell in an intact (*A*), mAbs-blocked (*B*), or TNF-α-stimulated (*C*) case. Data were presented as the histograms at a given cycle period $T = 18$ s together with the predictions (*lines*) fitted using a Gaussian equation.

returned the predicted mean value of $x_0 = 21.5$–$29.7$, 19.6–27.2, and 22.1–27.0 μm$^2$ for contact area, or $x_0 = 2.74$–$22.4$, 2.43–18.8, and 2.55–24.6 s for contact duration (Table 1; Table S1; Table S2). Again, the predictions $x_0$ were in agreement with those measured mean values of $A_c$ or $T_c$.

### 3.4. Parametric analysis of gas flux and medium viscosity

While it is well known how the suction pressure affects the contact and retraction of the two apposed cells in a conventional MAT assay (Huang et al., 2004; Wu et al., 2007; Long et al., 2001), the impact of gas-driven impinge pressure remains unclear for cell approach to and contact with the apposed cell, which in turn determines the fate of each contact event. To test its function, the impinge pressure was systematically varied by a gas flux of 150, 175, and 200 ml/min and the approaching velocity, apparent contact area, contact duration, and adhesion probability were compared for a Jurkat cell interacting with a MDA-MB-231 cell. Data indicated that the approaching velocity increased with gas flux, as expected, but yielded similar values in three cycle periods of $T = 12$, 15, and 18 s, even though the slight difference was found between those at $T = 15$ and 18 s at 150 ml/min or at $T = 12$ and 15 s at 175 ml/min ($P < 0.05$) (Fig. 7A). Similarly, the contact area also retained the stable values with varied gas flux and cycle period. As seen in Fig. 7B, although the contact area increased slightly from 150 to 175 ml/min at $T = 12$ s and was higher at 175 ml/min at $T = 12$ s than those at $T = 15$ and 18 s, it remained indifferent under three gas fluxes at long period of 15 or 18 s. This short period-related feature was mainly because the impingement of the two cells may not be saturated at the short contact duration and requires the high gas flux to reach equilibrated contact, whereas the high flux of ≥175 ml/min is sufficient to maintain the steady impingement at the longer contact duration. As a consequence, the contact duration slightly increased with gas flux at each given cycle period and presented the difference between the limited paired comparisons at distinct gas fluxes (Fig. 7C). Moreover, the resulting adhesion probability at each given gas flux increased with the cycle period mainly because of the prolonged contact duration but it retained the similar values at distinct gas fluxes at each given cycle period, except one higher adhesion probability at 200 ml/min than that at 150 ml/min at $T = 18$ s. Taken together, these results suggested that the adhesion probability increases with both gas flux and cycle period to reach the equilibrium binding at gas flux ≥175 ml/min at cycle period ≥15 s in the current experimental settings.

The viscosity of cell suspension varies in many pathophysiological processes such as blood high viscosity syndrome. It also governs the biophysics of cell–cell interactions to define if this process is shear-stress or shear-rate dependent (Alon et al., 1998). To test the potential effects, the medium viscosity was manipulated by adding highly viscous Percoll solution into the medium at a final concentration of 6% or 12%, which yields the maximized relative increase in dynamic viscosity of 14.0% or 24.5% at the lowest shear rate of 5 s$^{-1}$. At the given two high viscosities, the approaching velocity was reduced slightly in a relative decrease of 2.2–6.6% at two cycle periods of 12 and 15 s (Fig. 8A). By contrast, similar values were retained for the apparent contact area of 18.7–20.2 μm$^2$ (Fig. 8B). Contact duration was also indifferent in the values of 3.9–4.0 or 5.5–6.0 s, which yields the adhesion probability of 18–22% or 56–61%, at the respective cycle period of 12 (Fig. 8C) and 15 s (Fig. 8D). Thus, the dynamics of cell movement, contact, and adhesion are not affected by medium viscosity that varied in the current experimental settings.

## 4. Discussions

The goal of the current study is to elucidate the cell movement inside a pipette and cell contact with its counterpart cell sucked by another

**Table 1**
$U_f$ or $U_w$ and $A_c$ or $T_c$ distributions for an intact hPMN to a MDA-MB-231.

| Cycle period $T$ (s) | $U_f$ (μm/s) | | | | $U_w$ (μm/s) | | | | $A_c$ (μm$^2$) | | | | $T_c$ (s) | | | |
|---|---|---|---|---|---|---|---|---|---|---|---|---|---|---|---|---|
| | $R^2$ | $y_0$ | $x_0$ | σ | $R^2$ | $y_0$ | $x_0$ | σ | $R^2$ | $y_0$ | $x_0$ | σ | $R^2$ | $y_0$ | $x_0$ | σ |
| 8 | 0.91 | 0.19 | 37.1 | 15.6 | 0.82 | 0.26 | 27.6 | 9.70 | 1.00 | 0.46 | 25.6 | 5.99 | 0.95 | 0.47 | 2.74 | 1.11 |
| 10 | 0.99 | 0.28 | 31.4 | 10.0 | 0.91 | 0.19 | 29.7 | 14.2 | 0.77 | 0.16 | 29.2 | 19.2 | 0.96 | 0.32 | 4.12 | 1.64 |
| 12 | 1.00 | 0.55 | 30.1 | 5.10 | 0.87 | 0.25 | 40.0 | 11.3 | 0.98 | 0.41 | 28.4 | 6.36 | 0.99 | 0.42 | 5.18 | 1.36 |
| 15 | 0.72 | 0.25 | 31.0 | 12.0 | 0.66 | 0.20 | 36.6 | 13.8 | 0.96 | 0.38 | 29.7 | 6.95 | 0.78 | 0.38 | 9.31 | 1.05 |
| 18 | 0.99 | 0.57 | 24.3 | 4.62 | 0.94 | 0.33 | 43.0 | 7.61 | 0.94 | 0.33 | 21.5 | 8.51 | 0.95 | 0.31 | 10.4 | 1.81 |
| 22 | 0.84 | 0.22 | 30.5 | 12.1 | -† | -† | -† | -† | 0.89 | 0.38 | 23.0 | 7.13 | 0.55 | 0.11 | 12.8 | 5.52 |
| 26 | 0.98 | 0.28 | 26.0 | 9.81 | 0.86 | 0.18 | 41.4 | 15.1 | 1.00 | 0.43 | 24.5 | 6.55 | 0.97 | 0.18 | 18.4 | 2.94 |
| 31 | 0.84 | 0.40 | 20.6 | 5.41 | 0.52 | 0.29 | 28.3 | 6.3 | 0.90 | 0.41 | 27.6 | 6.42 | 0.71 | 0.10 | 22.4 | 5.47 |

All the histograms were fitted using a Gaussian distribution: $y = y_0 \times \exp.\{-[(x\text{-}\ x_0)/\sigma]^2\}$.
† : Note that $U_w$ data at cycle period $T = 18$ s is not able to fit using Gaussian distribution since there is an extremely high fraction at maximum values of $U_w$.

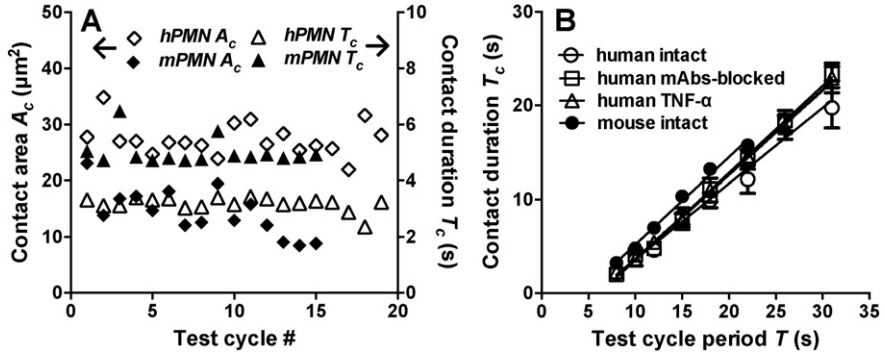


**Fig. 5.** Stability of apparent contact area and contact duration. Dependence of apparent contact area $A_c$ (*diamonds*) and contact duration $T_c$ (*triangles*), on consecutive cycles at a typical cycle period of $T = 10$ s when a hPMN (*open points*) or a mPMN (*solid points*) approaches to or withdraws from a MDA-MB-231 cell or a LSEC cell (*A*). Also plotted was the dependence of mean contact duration on cycle period for three cases of the binding of an intact (*open cycles*) or mAbs-blocked (*open squares*) hPMN to a MDA-MD-231 cell, and of an intact hPMN to a TNF-α-stimulated MDA-MD-231 cell (*open triangles*), as well as for one case of the binding of an intact mPMN to a LSEC cell (*solid cycles*) (*B*).

pipette. Our previous GDMAT assay that has been used for measuring the contact duration dependence of adhesion probability for two nucleated cells (Fu et al., 2011) was further extended here to systematically analyze the approaching or retraction velocity and contact area or duration. These results provide the deeper insight to the dynamics of cell movement and contact in microvasculature.

Understanding the movement and contact of a nucleated cell is biologically relevant since most of cellular adhesive receptors and ligands are expressing on the surface of a nucleated cell. Multiple microvilli are usually presented on cell surface, which is able to induce the jerkiness of the freely-moving cell inside a blood vessel. Moreover, the formation of membrane tether in an adhesive event may also delay the relaxation and then slow down the retraction velocity after the cell is withdrawn away from the counterpart cell. Once the moving cell adheres to the steadily sucked counterpart cell and forms a tether between them, it could be withdrawn slowly at low velocity until the tether is collapsed. In the case of cell–cell binding without tether formation, however, the moving cell stays for a while at the adhering position after suction pressure $\Delta p^w$ is onset, followed by an accelerating phase to reach the free-flow velocity after the interacting bonds are broken up. Nevertheless, these factors seemed not to affect cell movement inside a smooth glass pipette, as observed that $U_f$ and $U_w$ do not vary with test cycles statistically (Fig. 3). Although quite a few of $U_f$ and $U_w$ values are binomially distributed at specific cycle periods, the global feature of cell movement inside the pipette lies in that the velocities are distributed normally by fitting well a Gaussian equation (Fig. 4; Table 1; Table S1; Table S2).

It should be noted that the dynamics of cell movement and contact with another cell inside the pipette is also associated with acting forces of the two cells. The impinging or pulling force $F$ acting on a static cell inside a pipette with a pressure drop ($\Delta p$) is, $F = \Delta p \pi R_p^2 (1 - 4\varepsilon/3R_p)$ where ε is the gap width between the cell and the pipette wall (Shao and Xu, 2002; Shao et al., 1998). Note that this solution is not accurate under our experimental conditions when a cell is positioned close to the pipette tip (Fig. 1). A finite element simulation was applied to quantify the effect of the gap distance, indicating a decreased pressure drop inside the pipette (from 98% to 60% when the gap changes from 2 to 0.5 μm on the chosen parameters) (Chen et al., 2010). Since the cell on the right side reported here has the smaller size than the one used in the reference (Chen et al., 2010), it is reasonably supposed that the actual pressure drop is ~80–90% of the original pressure drop and that the above equation is still applicable for force and cell movement calculations. Here the suction pressure was given to be 0.3 mm $H_2O$ and the gas flow rate was varied from 150 to 200 ml/min. As an example, the gas flux of 200 ml/min was calibrated to a positive pressure of 0.5 mm $H_2O$ and the impinging force applied on PMN was estimated to be 99 pN and the pulling force was to be 149 pN.

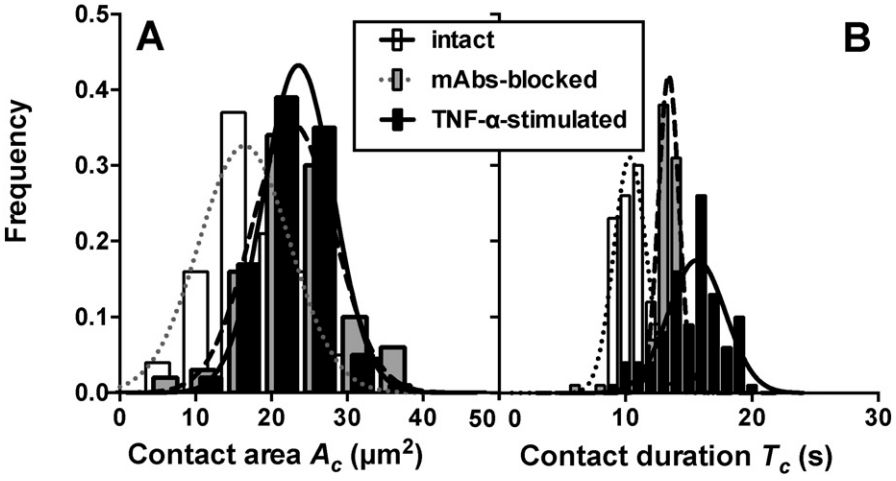


**Fig. 6.** Distributions of contact area and contact duration at given periods. Typical distributions of cell contact area $A_c$ (*A*) or contact duration $T_c$ (*B*) when a hPMN approaches to or withdraws from a MDA-MB-231 cell in an intact (*open bars* and *dotted lines*), mAbs-blocked (*gray bars* and *dashed lines*), or TNF-α-stimulated (*solid bars* and *solid lines*) case. Data were presented as the histograms at a given cycle period $T = 18$ s together with the predictions (*lines*) fitted using a Gaussian equation.

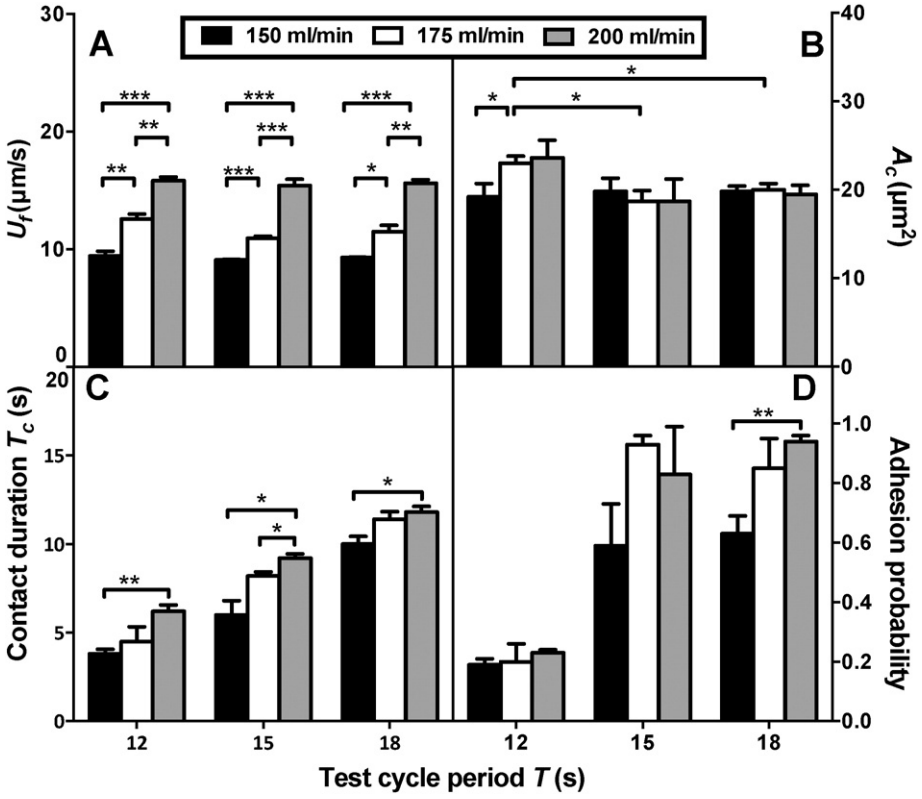


**Fig. 7.** Parametric analysis of gas flux. Dependence of approaching velocity (*A*), contact area (*B*), contact duration (*C*), and adhesion probability (*D*) of a flowing Jurkat cell to a sucked MDA-MB-231 cell on varied gas flux of 150, 175, and 200 ml/min at three typical test cycle periods of 12 (*black bars*), 15 (*white bars*), or 18 s (*gray bars*). Data were measured for ≥3 cell pairs and presented as the mean ± standard error (SE).

A robust GDMAT assay is biologically significant, not only for quantifying the binding kinetics of physiological receptors and their ligands constitutively expressed onto two nucleated cells (Fu et al., 2011) but also for monitoring the cell movement or jerkiness, compression, and relaxation in a size-limited pipette. For example, no matter if the two cells (i.e., a hPMN and a MDA-MB-231 cell) are intact (native), down-regulated ($\beta_2$-integrin blocked), or up-regulated (TNF-α-stimulated), the assay is sufficiently stable to quantify their movement, contact, and adhesion. Together with the medium viscosity-independent data (Fig. 8), these results also implied that the cell movement and contact is shear-rate dependent, at least, in the current experimental setting, supporting the previous observations that cell transportation under shear flow is governed by shear rate (Liang et al., 2008; Chen and Springer, 2001). Therefore, future technical improvements in such the high-speed image grabbing, the automatic image digitalization and displacement calculation, the high-quality pressure regulator for ultra-stable gas flow (Dufour and Toure, 2004), and the delicate pipette pre-treatment for free of non-specific binding (Sundd et al., 2008) could further extend this assay to test the impacts of impinge force, pulling force, tether formation and force, and cell stiffness and microtopology to mimic in vitro the PMN movement and adhesion inside a blood vessel. Besides, it could also be used to monitor in situ intracellular signaling of the moving cell when combined with specific fluorescence probes.

## 5. Conclusion

In this study, we quantified the impact of those regulating factors on cell movement, contact, and adhesion in a novel GDMAT assay. Our analyses presented the independence in consecutive test cycles between approaching and retraction velocity or between contact area and duration, providing an applicable approach for continuously monitoring cell movement and contact events inside a pipette. Cell–cell adhesion reaches equilibrium with increased contact duration and the adhesion is not affected by medium viscosity varied in the current experimental settings. These data imparted the confidence that GDMAT assay is robust in determining the movement, contact and adhesion between two nucleated cells.

*Abbreviations*

| | |
|---|---|
| RBC | Red blood cell |
| LSECs | Liver sinusoidal endothelial cells |
| GDMAT | Gas-driven micropipette aspiration technique |
| PMN | Polymorphonuclear neutrophil |
| HPMEC | Human pulmonary microvascular endothelial cell |
| WM9 | Human melanoma cell line |
| MDA-MB-231 | Human breast cancer cell line |
| ICAM-1 | Intercellular adhesion molecule 1 |
| mAbs | Monoclonal antibodies |
| APC | Allophycocyanin |
| FITC | Fluorescein isothiocyanate |
| FBS | Fetal bovine serum |
| HBSS | Hank's Balanced Salt Solution |
| HEPES | 4-(2-Hydroxyethyl)piperazine-1-ethanesulfonic acid |
| D-PBS | Dulbecco's Phosphate-Buffered Saline |
| HSA | Human serum albumin |
| TNF-α | Tumor-necrotic factor alpha |
| NPCs | Non-parenchymal cells |
| EGTA | Ethylene glycol tetraacetic acid |
| DMEM | Dulbecco's modified Eagle's medium |
| BSA | Bovine serum albumin |

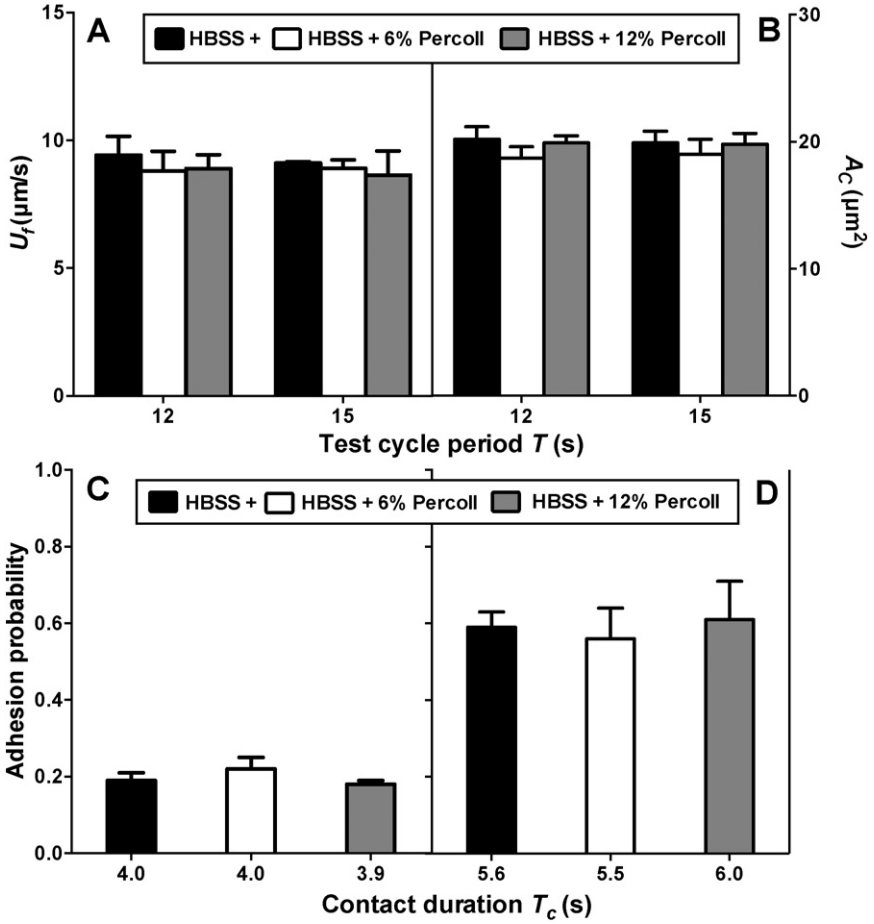


**Fig. 8.** Parametric analysis of medium viscosity. Dependence of approaching velocity (*A*), contact area (*B*), and adhesion probability (*C*, *D*) of a flowing Jurkat cell to a sucked MDA-MB-231 cell on varied medium viscosity in the absence (*black bars*) or presence of 6% (*white bars*) and 12% (*gray bars*) Percoll mixture at two typical test cycle periods of 12 (*C*) and 15 s (*D*). Data were measured for ≥3 cell pairs and presented as the mean ± SE.

## Conflict of interest

The authors declare no competing financial interests.

## Authorship

ML and YZ, SL and NL conceived the research; ML designed the experiments and wrote the paper; HY analyzed the data and wrote the paper; CT performed the cell adhesion experiments and wrote the paper; CF developed the GDMAT technique; XL conducted the Pearson correlation analysis; YX and QC analyzed the data. All authors read and approved the final manuscript.

## Acknowledgments

This work was supported by the National Natural Science Foundation of China grants 31230027 and 31110103918, National Key Basic Research Foundation of China grant 2011CB710904, and Strategic Priority Research Program of Chinese Academy of Sciences grant XDA01030102.

## Appendix A. Supplementary data

Supplementary data to this article can be found online at http://dx.doi.org/10.1016/j.jim.2015.11.007.

## References

Alon, R., Chen, S., Fuhlbrigge, S.R., Puri, K.D., Springer, T.A., 1998. The kinetics and shear threshold of transient and rolling interactions of L-selectin with its ligand on leukocytes. Proc. Natl. Acad. Sci. U. S. A. 95, 11631–11636.

Chen, S.Q., Springer, T.A., 2001. Selectin receptor-ligand bonds: formation limited by shear rate and dissociation governed by the Bell model. Proc. Natl. Acad. Sci. U. S. A. 98, 950–955.

Chen, W., Lou, J.Z., Zhu, C., 2010. Forcing switch from short- to intermediate- and long-lived states of the alpha a domain generates LFA-1/ICAM-1 catch bonds. J. Biol. Chem. 285, 35967–35978.

Chesla, S.E., Selvaraj, P., Zhu, C., 1998. Measuring two-dimensional receptor–ligand binding kinetics by micropipette. Biophys. J. 75, 1553–1572.

Dufour, P., Toure, Y., 2004. Multivariable model predictive control of a catalytic reverse flow reactor. Comput. Chem. Eng. 28, 2259–2270.

Fu, C.L., Tong, C.F., Wang, M.L., Gao, Y.X., Zhang, Y., Lü, S.Q., Liang, S., Dong, C., Long, M., 2011. Determining beta2-integrin and intercellular adhesion molecule 1 binding kinetics in tumor cell adhesion to leukocytes and endothelial cells by a gas-driven micropipette assay. J. Biol. Chem. 286, 34777–34787.

Gelles, J., Schnapp, B.J., Sheetz, M.P., 1988. Tracking kinesin-driven movements with nanometre-scale precision. Nature 331, 450–453.

Huang, J., Chen, J., Chesla, S.E., Yago, T., Mehta, P., McEver, R.P., Zhu, C., Long, M., 2004. Quantifying the effects of molecular orientation and length on two-dimensional receptor–ligand binding kinetics. J. Biol. Chem. 279, 44915–44923.

Langlois, W., Deville, M., 2014. Exact Solutions to the Equations of Viscous Flow. Slow Viscous Flow. Springer International Publishing, pp. 105–143.

Ley, K., 2003. The role of selectins in inflammation and disease. Trends Mol. Med. 9, 263–268.

Li, N., Mao, D.B., Lü, S.Q., Tong, C.F., Zhang, Y., Long, M., 2012. Distinct binding affinities of Mac-1 and LFA-1 in nerophil activation. J. Immunol. 190, 4371–4381.

Liang, S., Dong, C., 2008. Integrin VLA-4 enhances sialyl-Lewis(x/a)-negative melanoma adhesion to and extravasation through the endothelium under low flow conditions. Am. J. Physiol. Cell Physiol. 295, C701–C707.

Liang, S.L., Fu, C.L., Wagner, D., Guo, H.G., Zhan, D.Y., Dong, C., Long, M., 2008. Two-dimensional kinetics of beta(2)-integrin and ICAM-1 bindings between

neutrophils and melanoma cells in a shear flow. Am. J. Physiol. Cell Physiol. 294, C743–C753.
Long, M., Goldsmith, H.L., Tees, D.F.J., Zhu, C., 1999. Probabilistic modeling of shear-induced formation and breakage of doublets cross-linked by receptor-ligand bonds. Biophys. J. 76, 1112–1128.
Long, M., Zhao, H., Huang, K.S., Zhu, C., 2001. Kinetic measurements of cell surface E-selectin/carbohydrate ligand interactions. Ann. Biomed. Eng. 29, 935–946.
Mansson, R., Tsapogas, P., Akerlund, M., Lagergren, A., Gisler, R., Sigvardsson, M., 2004. Pearson correlation analysis of microarray data allows for the identification of genetic targets for early B-cell factor. J. Biol. Chem. 279, 17905–17913.
Shao, J.Y., Xu, J.B., 2002. A modified micropipette aspiration technique and its application to tether formation from human neutrophils. J. Biomech. Eng. -T Asme 124, 388–396.
Shao, J.Y., Ting-Beall, H.P., Hochmuth, R.M., 1998. Static and dynamic lengths of neutrophil microvilli. Proc. Natl. Acad. Sci. U. S. A. 95, 6797–6802.
Sun, G.Y., Zhang, Y., Huo, B., Long, M., 2009a. Surface-bound selectin-ligand binding is regulated by carrier diffusion. Eur. Biophys. J. Biophys. 38, 701–711.
Sun, G.Y., Zhang, Y., Huo, B., Long, M., 2009b. Parametric analysis for monitoring 2D kinetics of receptor–ligand binding. Cell. Mol. Bioeng. 2, 495–503.
Sundd, P., Zou, X.Y., Goetz, D.J., Tees, D.F.J., 2008. Leukocyte adhesion in capillary-sized P-selectin-coated micropipettes. Microcirculation 15, 109–122.
Tees, D.F.J., Goldsmith, H.L., 1996. Kinetics and locus of failure of receptor–ligand-mediated adhesion between latex spheres.1. Protein–carbohydrate bond. Biophys. J. 71, 1102–1114.
Wu, L., Xiao, B.T., Jia, X.L., Zhang, Y., Lü, S.Q., Chen, J., Long, M., 2007. Impact of carrier stiffness and microtopology on two-dimensional kinetics of P-selectin and P-selectin glycoprotein ligand-1 (PSGL-1) interactions. J. Biol. Chem. 282, 9846–9854.